Modeling adaptive cruise control vehicles from experimental data: model comparison

George Gunter, Raphael Stern, *Member, IEEE*, and Daniel B. Work, *Member, IEEE*

***Abstract*— This article uses experimentally collected car following data from seven different commercially available *adaptive cruise control* (ACC) vehicles to calibrate microscopic models for each system's car following behavior using three different common car following models. Calibration is conducted by selecting the model parameters that minimize the error between the simulated vehicle trajectories and the experimental data. The goal of this study is two-fold: (*i*) assess which car-following models typically used to describe human driving behavior are best for describing ACC car-following dynamics, and (*ii*) provide best-fit calibrated car following models for seven different commercially available ACC vehicles, which can be used to understand the traffic flow impact of ACC systems via simulation analysis. We find that the intelligent driver model and the optimal velocity model with a relative velocity term perform best, and with similar performance to one another, while the Gazis-Herman-Rothery model as calibrated does not capture all the ACC car following dynamics.**

I. Introduction

The emergence of *autonomous vehicles* (AVs) on highways and urban roadways has the potential to substantially impact traffic flow [1]–[3]. This is true not only for fully autonomous vehicles such as *Society of Automotive Engineers* (SAE) Level 5 AVs [4], but also vehicles with driver assist features (SAE Level 1 and 2 AVs) such as *adaptive cruise control* (ACC), which have been shown to be able to change the emergent properties of the traffic flow even at low AV penetration rates [1], [2], [5].

While fully autonomous vehicles may not be commercially-available for several more years, driver assist vehicles such as ACC have already become common place in many modern, commercially-available vehicles. With this in mind, it is important to be able to accurately model the car following behavior of ACC. This will be important for understanding how ACC vehicles may influence the traffic flow.

To model traffic flow at the level of the individual vehicle (microscopically), car following models are commonly used to describe the acceleration of a vehicle as a function of measurements from the vehicle's surroundings, which often consists of information about the next vehicle ahead in the traffic flow. This modeling approach dates back to experimental work conducted at General Motors in the 1950s [6]–[8], and generally takes the form:

$$\ddot{x}(t) = f(s(t), v(t), \Delta v(t)), \tag{1}$$

where $s(t)$ is the inter-vehicle space gap or space-gap, $v(t)$ is the speed of the following vehicle, and $\Delta v(t)$ is the relative velocity between the lead vehicle and the following vehicle, which are all time varying. The function $f(s(t), v(t), \Delta v(t))$ then describes the acceleration of the following vehicle as a function of these variables. To simplify the notation, we will omit the time index of most models. Using models of this form, it is possible to model both human-driver behavior as well as the vehicle-level dynamics of ACC vehicles [9]–[11].

Fundamental to calibrating such models is the collection of high-quality experimental field data that measures the trajectory of each individual vehicle. This has been the focus of several important works and is still highly relevant today as AVs and partially autonomous vehicles begin to enter our roadways and alter the traffic flow. Beyond the work at General Motors in the 1950s [6]–[8] other pioneering data collection efforts includes work done by Triterer in the 1970s, which involved flying a helicopter over freeways in Ohio to photograph traffic to reconstruct vehicle trajectories [12]. Perhaps the most widely used vehicle-level dataset is the the NGSIM data that was collected by placing video cameras on a 900 m section of I-80 in California. Also notable is the data collected by Gorte, *et al.* [13], where a helicopter was flown over Dutch freeways to collect vehicle trajectories. All of these data collection efforts have collected experimental data of human driving behavior.

More recently, there has been renewed interest in understanding vehicle-level behavior, with a focus on mixed human and AV traffic. For example, prior work by Gunter, *et al.* [10], [11] collected experimental data from ACC vehicles to understand whether commercially available ACC vehicles were string stable, while the experimental work by Stern, *et al.* [2] showed that controlling just a small fraction of AVs in human-piloted traffic flow could change the emergent properties of the flow.

The focus of this article is to compare the performance of different microscopic traffic models to simulate car following behavior of commercially available ACC vehicles. This is done by calibrating prospective models using experimentally collected data. The contribution of this work is two-fold: (*i*) this study enables future theoretical works by exploring which car following models are best suited for modeling the dynamics of commercially available ACC systems, and (*ii*) this study provides best-fit calibrated car following models

G. Gunter and D. Work are with the Department of Civil and Environmental Engineering and the Institute for Software Integrated Systems, Vanderbilt University, TN (email: {guntergl, dan.work}@vanderbilt.edu).

R. Stern is with the Department of Informatics at the Technical University of Munich, Germany and the Department of Civil, Environmental, and Geo-Engineering at the University of Minnesota, MN (email: rstern@umn.edu).

for seven different commercially available ACC vehicles, which can be used to understand the traffic flow impact of ACC systems via simulation analysis. Importantly, this work does not consider a specific vehicle dynamical model, but instead calibrates a microscopic traffic model to the overall performance of the ACC vehicle, without considering the low-level controller that may be implemented on the vehicle. Instead, we describe the traffic-level performance of the vehicle, which is important to understand the impact of ACC vehicles on the traffic flow.

In previous publications by the authors [11] a single delay differential equation car following model was developed and fit to ACC following data and then assessed for string stability while in [10] a single car following model was calibrated for a high performance electric vehicle to assess string stability of the ACC system. The present work differs in that three common car following models are calibrated to compare the performance for modeling ACC following behavior of commercially available vehicles. The car following vehicle trajectory dataset used to calibrate the models in this article come from a series of field experiments that was originally published by Gunter, *et al.* [11] and contains over 1,000 miles of car following trajectories for seven different commercially available ACC vehicles.

The remainder of this article is outlined as follows: in Section II the three car following models used are reviewed: the *Gazis-Herman-Rothery* model (GHR) [8], the *intelligent driver model* (IDM) [14], and the *Optimal Velocity with Relative Velocity* model [9], [10]. The experimental data used to calibrate the models is presented in Section III, and the model calibration methodology is presented in Section IV. The results of the model calibration are presented in Section V, and we conclude that the OVRV model and IDM model perform roughly the same, and outperform the GHR model in Section VI.

II. Modeling ACC vehicle behavior

In this section, we briefly outline the general modeling framework used to model the car following behavior of the ACC vehicle, and then provide details on the specific car following models that are used in this article.

A. General modeling framework

The car-following behavior of an ACC vehicle may depend on many external factors such as the internal state of the engine, the current gear, and road grade, among others. However, modeling each of these components may not be necessary, or even desirable, when considering the vehicle-level car following behavior of an ACC vehicle. Instead, the vehicle-level dynamics may be more useful when trying to model ACC vehicles in the traffic flow. Therefore, this article considers the modeling approach used by Milanés and Shladover [9] as well as Gunter, *et al.* [10], [11] to use a differential equation to model the vehicle-level car following behavior. This differential equation can then be used as a proxy for the ACC car following dynamics and analyzed for theoretical properties such as string stability.

Specifically, in this article, we model the response of an ACC vehicle to a lead vehicle immediately in front of it. We assume that through the on-board sensors, the ACC vehicle is able to measure the space gap between the lead vehicle and the ACC vehicle s as well as its own speed v and the relative speed with respect to the lead vehicle Δv. Using these inputs, the acceleration of the ACC vehicle $\ddot{x}$ is modeled as a differential equation with the general form:

$$\ddot{x} = f(p, s, v, \Delta v), \tag{2}$$

where p is a vector of model parameters, s is the space gap, $v = \dot{x}(t)$ is the velocity of the follower, and $\Delta v := \dot{s}(t)$ is the relative velocity between the leader and follower. Next, we review three common car following models that will be considered in this article.

B. Gazis-Herman-Rothery model

One of the first commonly-used car following models is the GHR [8] car following model, which is one of the most widely-known car following models and originates from research conducted by General Motors in the 1950s. The model contains a delay term to account for human reaction time, but is considered to be the delay of the ACC system in this study. The model is therefore a delayed differential equation that takes the form:

$$\ddot{x}(t) = cv(t)^m \frac{\Delta v(t-T)}{s^\ell(t-T)}, \tag{3}$$

where c, m, and ℓ are model parameters, T is the delay, and all other terms are defined as before.

C. Intelligent driver model

The IDM [14] was developed by Treiber, Hennecke, and Helbing in 2000 and is one of the most widely used microscopic traffic models today. In the IDM, the acceleration function takes the form:

$$\ddot{x} = a\left(1 - \left(\frac{v}{v_0}\right)^\delta - \left(\frac{\hat{s}(v, \Delta v)}{s}\right)^2\right), \tag{4}$$

where

$$\hat{s}(v, \Delta v) = s_0 + \tau v - \max\left(0, \frac{v\Delta v}{2\sqrt{ab}}\right). \tag{5}$$

Here v_0 is the desired speed, which can be interpreted as the ACC setpoint speed, τ is the time headway, a is the maximum acceleration that the ACC vehicle can achieve, b is the maximum braking rate that the ACC vehicle can achieve, δ is a model parameter, and s_0 is the jam distance. The values of a and b should fall within the bounds that are prescribed in the relevant standards (e.g., ISO15622:2010 [15]).

D. Optimal velocity model with relative velocity term

One model, which has previously been used to model ACC vehicle dynamics [9], [10], is the *optimal velocity* (OV) model with a *relative velocity* term (OVRV):

$$\ddot{x}(t) = \alpha\left(V(s) - v\right) + \beta\left(\Delta v\right). \tag{6}$$



Fig. 1. Experimental setup with lead vehicle in front of following vehicle on straight, flat track. Note that the images are blurred to obscure vehicle make and model.

In the above model (6), the first component relaxes the follower velocity to a desired velocity prescribed by the *optimal velocity* function V based on the current space gap to the vehicle in front, while the second component relaxes the follower velocity to the velocity of the leader. The model parameters α and β control the tradeoffs between following the optimal velocity and following the leader velocity.

For the purposes of modeling adaptive cruise control vehicles, we adopt a special case of the OVRV model (6) considered in [3], [10], [11], [16], [17]:

$$\ddot{x} = k_1(s - \eta - \tau v) + k_2(\Delta v) \tag{7}$$

where k_1 and k_2 are the gain parameters on the constant time-headway term and a follow-the-leader term respectively, η is the jam space gap (the minimum distance two vehicles will attain) and the parameter τ is the desired headway. Note that the model (7) operates under a linear optimal velocity function $V(s) := s/\tau$ and with $\alpha := k_1\tau$. It is considered a constant time-headway term because the space gap s is adjusted based on the speed such that the headway τ is maintained. It is well known that constant time-headway based controllers are important to overcome the inherent limitations of linear controllers to achieve a string stable constant space gap policy and is often assumed for commercial ACC vehicles [18].

III. Experimental data

The experimental data used in this study is collected by, and presented in the article by Gunter, *et al.* [11]. The dataset consists of car following vehicle trajectories from seven different modern, commercially available ACC vehicles. The data contains over 1,900 km of car following data ranging from speeds of roughly 55 km/h to 110 km/h on flat ground. The experiments are briefly described below for completeness. For a full description of the experimental methods, please see the article by Gunter, *et al.* [11].

Each experiment is conducted with a lead vehicle driving a consistent, pre-determined speed profile, and the following vehicle driving behind the lead vehicle with ACC engaged. The vehicles are arranged on a straight, flat track as shown in Figure 1 with the lead vehicle in front of the following vehicle. Position and speed data are collected from each vehicle using a high-resolution GPS sensor.

Vehicle	Style	Engine type
A	Full-size sedan	Combustion
B	Compact sedan	Combustion
C	Compact hatchback	Hybrid
D	Compact SUV	Combustion
E	Compact SUV	Combustion
F	Mid-size SUV	Combustion
G	Full-size SUV	Combustion

TABLE I

Summary of tested vehicles.

Each vehicle is tested both at the minimum (closest) and the maximum (furthest) following settings to acquire an understanding for the range of car following behaviors that the vehicle may exhibit under ACC driving. Each vehicle is driven in four different experiments at each following setting for a total of roughly 130 km (80 miles) of driving for each vehicle. These tests are designed to include steady state and transient behavior over a range of speeds from 15.6 m/s (35 mph) to 33.5 m/s (75 mph). Thus, in total, these experimental data represent over 1000 km (620 miles) of car following data.

The seven vehicles tested range in size from a small compact hybrid electric hatchback to a large, fill-size SUV. An overview of the tested vehicles is provided in Table I.

IV. Model calibration

In this section the calibration of the different models is explained. For each model the optimal model parameters that produce the smallest error with respect to the experimental data are found by by solving a simulation based optimization problem. Here each potential model is compared against the data, and an error metric is calculated to describe its goodness of fit. In this work, all models are calibrated according to the *root mean squared error* (RMSE) in between simulated speed data and recorded speed data. The general optimization scheme can be formulated as follows:

$$\begin{aligned} \underset{s,v,\Delta v,p}{\text{minimize :}} \quad & \sqrt{\tfrac{1}{T}\int_0^T (v_{\text{m}}(t) - v(t))^2 dt} \\ \text{subject to:} \quad & \dot{v}(t) = f(p, s, v, \Delta v) \\ & \dot{s}(t) = v_{l,\text{m}}(t) - v(t) \\ & s(0) = s_{\text{m}}(0) \\ & v(0) = v_{\text{m}}(0) \\ & \Delta v(0) = \Delta v_{\text{m}}(0) \\ & p \geq U \\ & p \leq L \end{aligned} \tag{8}$$

where s, v, and Δv are the ACC vehicle space gap and speed, and speed difference between the ACC vehicle and a leading vehicle. The variable p refers to the vector of model parameters, where $f(p, s, v, \Delta v)$ is a model that describes how the speed of the vehicle changes. In the case of the OVRV, IDM, and GHR models these are explicit differential equations on the acceleration, which must be integrated to determine speed and space gap values. The terms $s_{\text{m}}(0)$, $v_{\text{m}}(0)$ and $\Delta v_{\text{m}}(0)$ refer to initial conditions on the speed, space gap, and speed difference for the following vehicle, and

$v_{l,\mathrm{m}}$ is the lead vehicle speed. In addition to the constraints on the initial conditions, for some of the models it is desirable to constrain the range over which the parameters values (p) can vary. As such the optimization scheme is a constrained one in which potential lower bound L and upper bound U are placed on the parameters, p. Note that this implies that p, L an U are vectors that all have the same length.

The parameter values for each of the models are calibrated for each of the seven vehicles (A-G) at each of the two tested following settings (minimum and maximum). Thus, a total of 14 sets of best-fit parameter values are calibrated for each of the three tested car following models. To calibrate each of the models, data from three of the tests are used as training data, and data from the fourth test are reserved as a hold-out test set to evaluate the model performance on data that were not used to calibrate the model.

In the case of the GHR model, to expedite computational time since it is a delay differential equation, the model is calibrated using a two-step process where first the model parameters c, m, and ℓ are calibrated using (8) without considering the impact of the delay. Next, a parameter sweep in the neighborhood of the optimal model parameter values is conducted to find the best-fit delay differential equation parameter values that consider the delay T. While this does not guarantee the best fit model globally, this methodology is adopted since calibrating the delay differential equation in one step using (8) was found to be extremely computationally demanding. Specifically, the calibration of a single model took over 120 hours of computation time on a 16-core computer.

V. Results

In this section the calibrated model parameters are presented, and the relative performance of each model for each vehicle is discussed and compared. Model parameter values are calibrated for acceleration in units of m/s^2, velocity in units of m/s, and space gap in units of m.

The training error for the best-fit model for both speed and space gap are shown in Figure 2 and Figure 3, respectively. Here the performance for the calibrated model for each of the seven vehicles (A-G) at each of the two following settings tested (minimum and maximum) are presented separately for each of the three car following models (GHR, IDM, and OVRV). The average errors are presented in Table II. The OVRV and IDM have the same average speed error across all vehicles with a train RMSE of 0.27 m/s. The OVRV has the lowest space gap train error with an RMSE of 2.51 m. The GHR has the greatest training error with a speed RMSE of 0.38 m/s and a space gap RMSE of 7.11 m. However, note that this higher training error may be in part because the GHR is a delay differential equation, and thus a different training routine was used to calibrate the model. To give a sense of the quality of fit, the model performance of each best-fit model for Vehicle B is shown in the example speed plot in Figure 4. Here one of the training datasets is used as the lead vehicle trajectory, and the actual following vehicle data as well as the simulated following vehicle using each of the three calibrated models for Vehicle B at the minimum following setting is shown.

Model	Speed train (m/s)	Speed test (m/s)	Space gap train (m)	Space gap test (m)
GHR	0.38	0.74	7.11	8.79
IDM	0.27	0.41	4.00	4.23
OVRV	0.27	0.46	2.51	4.10

TABLE II
AVERAGE TRAIN AND TEST RMSE FOR EACH MODEL.



Fig. 2. Relative comparison of the speed RMSE on the training data for each model.

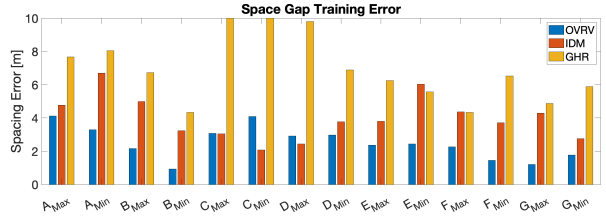


Fig. 3. Relative comparison of the space gap RMSE on the training data for each model.

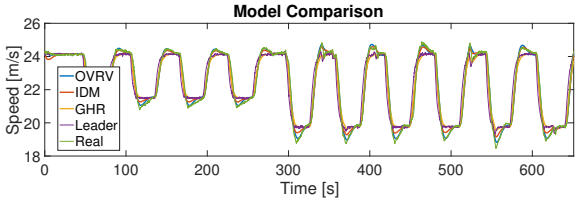


Fig. 4. Comparison of models for Vehicle B, minimum following setting.

The calibrated model parameters for each vehicle and each model are presented in Table III. To better interpret the results, they are also graphically displayed in Figures 5 through 7.

As seen in Figure 5 for the GHR model, the calibrated parameters values for c range from roughly 0 to 8, while the values for m range from roughly -1.5 to 1, the values for ℓ range between -1.5 and 1, with the majority of the values between 0.5 and 1, and the values for T range from 0.8 s to 1.5 s. Note that c, m, and ℓ are all unitless, but calibrated for SI units as inputs. In terms of the parameter value distribution, with the models calibrated for the maximum following setting having smaller values of c than models calibrated for the minimum following setting and larger values for the delay in the differential equation T generally corresponding to the maximum following setting. The calibrated parameter values for m and ℓ do not show a clear pattern with respect to the following setting.

As seen in Figure 6 for the IDM as well as in Table III, the model parameter values for V_0 range from roughly 30

Vehicle	Setting	GHR				IDM						OVRV			
		c [-]	m [-]	ℓ [-]	T [s]	V_0 [m/s]	τ [s]	s_0 [m]	δ [-]	a [m/s^2]	b [m/s^2]	k_1 [s^{-2}]	k_2 [s^{-1}]	τ [s]	η [m]
A	Minimum	7.57	-0.54	0.35	1.03	37.26	0.76	19.95	155.12	0.79	3.50	0.04	0.18	0.60	17.74
A	Maximum	0.09	0.86	0.38	1.43	36.5	1.65	20.00	155.34	0.67	3.50	0.02	0.13	1.71	21.51
B	Minimum	3.86	-0.8	-0.13	1.23	33.51	0.83	16.19	151.05	1.13	3.50	0.07	0.25	0.87	12.3
B	Maximum	0.02	-1.32	-1.69	1.5	33.97	2.00	15.57	154.08	0.81	3.13	0.02	0.16	1.84	16.04
C	Minimum	0.85	0.69	0.85	0.77	44.34	0.76	15.89	154.52	0.48	3.50	0.02	0.24	0.31	28.42
C	Maximum	0.22	0.82	0.61	1.36	45.45	1.90	15.98	155.64	0.53	3.44	0.01	0.15	1.84	20.52
D	Minimum	5.99	-0.30	0.49	1.14	41.3	0.71	18.90	154.76	0.75	3.50	0.04	0.21	0.63	16.64
D	Maximum	0.52	0.16	0.30	1.39	46.90	1.85	16.13	155.02	0.68	3.50	0.02	0.15	1.98	13.20
E	Minimum	2.58	-0.75	-0.13	1.07	40.63	1.13	13.99	154.68	1.02	3.50	0.06	0.11	1.50	1.08
E	Maximum	0.84	-0.6	-0.23	1.25	46.11	1.66	20.00	155.35	1.14	3.50	0.06	0.07	2.04	10.31
F	Minimum	0.79	0.08	0.22	1.18	50.00	0.00	20.00	1.06	2.00	3.50	0.06	0.17	0.79	12.88
F	Maximum	3.02	-0.73	0.00	1.21	48.81	1.45	20.00	154.88	0.87	3.50	0.05	0.09	2.04	3.31
G	Minimum	0.96	-0.59	-0.34	0.97	36.15	0.59	19.99	155.36	0.95	3.50	0.07	0.17	0.80	12.51
G	Maximum	1.94	-0.73	-0.11	0.88	38.87	1.51	19.3	154.49	0.88	3.50	0.05	0.10	2.06	4.17

TABLE III

CALIBRATED MODEL PARAMETER VALUES FOR ALL VEHICLES AND MODELS.

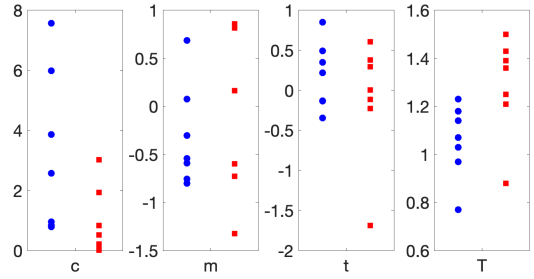


Fig. 5. Parameter values for IDM. Blue circles for minimum following setting models, red squares for maximum following setting models.

m/s to 50 m/s, the values for T range from 0 s to 2 s, the values for s_0 range from 14 m to 20 m, the values for δ are unitless and range from 0 to 160, the values for a range from 0.4 m/s^2 to 2 m/s^2, and the values for b range from 3.1 m/s^2 to 3.5 m/s^2. Note that the values for a and b were calibrated to fall within the required bounds prescribed by the relevant ISO 15622 standard of 2.0 m/s^2 and 3.5 m/s^2 as the maximum acceleration and braking, respectively [15]. No other parameters were constrained. The values for V_0, s_0, a, and b show no clear trend between the minimum and maximum following setting, while the values for T show that lower values correspond to the minimum setting model, and the values for δ show a clear outlier with the minimum following setting model for vehicle F being substantially lower than all other models.

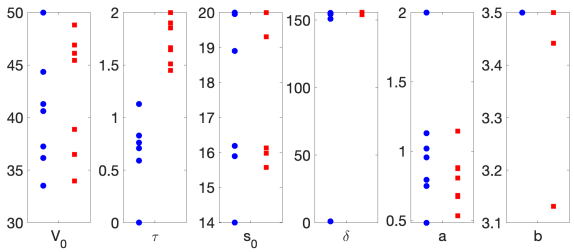


Fig. 6. Parameter values for IDM. Blue circles for minimum following setting models, red squares for maximum following setting models.

For the OVRV model, the resulting parameter values are presented in Table III and graphically displayed in Figure 7. The values for k_1 range between 0.01 s^{-2} and 0.08 s^{-2}, with smaller values typically corresponding to the maximum following setting model. The values for k_2 range from 0.05 s^{-1} to 0.25 s^{-1}, again with smaller values typically corresponding to the maximum following setting model. The values for τ range from 0.3 s to just over 2 s, with smaller values corresponding to the minimum following setting model, and the values of η range from roughly 1 m to nearly 30 m with values for both the minimum and maximum following setting model spread throughout that range.

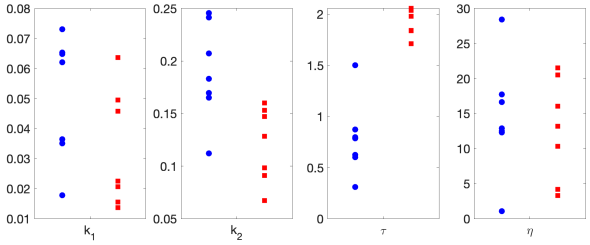


Fig. 7. Calibrated parameter values for OVRV model. Blue circles correspond to minimum following setting models, and red squares refer to maximum following setting models. See Table III for proper units.

The testing errors on the hold-out test set for speed and space gap are shown in Figure 9 and Figure 10, respectively, as well as in Table II. Overall, the IDM and the OVRV perform roughly the same with an average speed RMSE of 0.41 m/s and 0.46 m/s, respectively and an average space gap RMSE of 4.23 m and 4.10 m, respectively, while the GHR model generally has a higher average RMSE. However, again, it is possible that this is a result of the training routine used for the GHR, and it is possible that a better-fitting model could be found.

The model performance on the hold-out test data can bee seen in Figure 8 where the best-fit models for Vehicle A at the minimum following setting are simulated. As seen in Figure 8, the GHR model closely follows the lead vehicle speed, and therefore does not match the following vehicle dynamics. In contrast, the OVRV model and the IDM model are able to incorporate the fact that ACC vehicles are space gap-error based controllers and considered whether or not

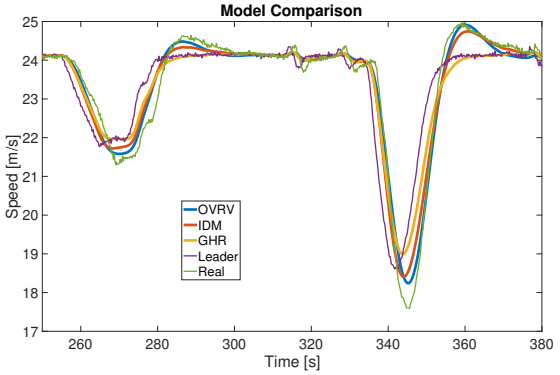


Fig. 8. Comparison of model responses for Vehicle B at the minimum following setting.

the vehicle is at the appropriate space-gap for a given speed. Thus, for practical modeling and analysis applications of ACC following behavior, the OVRV and IDM model are both suitable. Note that the IDM has the added benefit that it can be calibrated to explicitly take to take into account physical constraints on acceleration and braking.

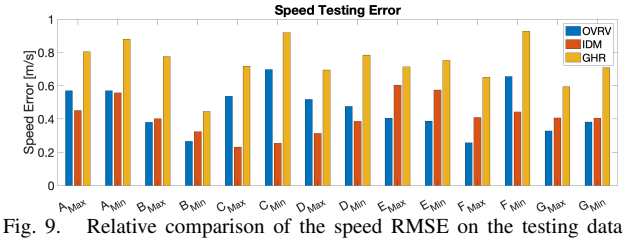


Fig. 9. Relative comparison of the speed RMSE on the testing data for each model.

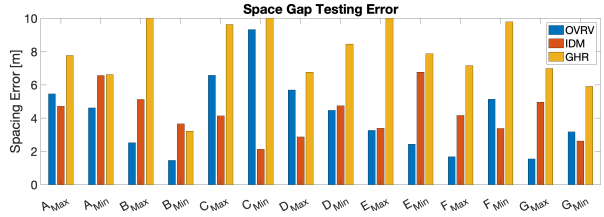


Fig. 10. Relative comparison of the space gap RMSE on the testing data for each model.

VI. Conclusions

In conclusion, the OVRV and IDM model both performed well in modeling the ACC following vehicle behavior, while the GHR model produced a higher speed and spacing RMSE. However, it is possible that a different calibration routine could yield GHR model parameters with a lower RMSE. The calibrated parameter values show that there is variability in ACC car following behavior across the vehicle fleet tested. These models can now be used to gain a better understanding of how ACC vehicles will influence traffic flow. This work goes beyond the prior work by comparing three different car following models for the purpose of modeling ACC vehicle following behavior. The resulting calibrated models represent the first set of calibrated car following models for a wide range of vehicles.

VII. Acknowledgements

This material is based upon work supported by the National Science Foundation under Grants No. CNS-1837652 (D.W. & R.S.) and OISE-1743772 (G.G.) as well as through the Federal Highway Administration's Dwight David Eisenhower Transportation Fellowship Program under Grant No. 693JJ31845050 (R.S). The authors would also like to acknowledge C. Janssen, Y. Wang, D. Gloudemans, and W. Barbour for assisting in data collection as well as the Vanderbilt VUSE Summer Research Program.

References

[1] A. Talebpour and H. S. Mahmassani. Influence of autonomous and connected vehicles on stability of traffic flow. In *Transportation Research Board 94th Annual Meeting*, number 15-5971, 2015.

[2] R. E. Stern, S. Cui, M. L. Delle Monache, R. Bhadani, M. Bunting, M. Churchill, N. Hamilton, R. Haulcy, H. Pohlmann, F. Wu, B. Piccoli, B. Seibold, J. Sprinkle, and D. B. Work. Dissipation of stop-and-go waves via control of autonomous vehicles: Field experiments. *Transportation Research Part C: Emerging Technologies*, 89:205 – 221, 2018.

[3] L. C. Davis. The effects of mechanical response on the dynamics and string stability of a platoon of adaptive cruise control vehicles. *Physica A: Statistical Mechanics and its Applications*, 392(17):3798–3805, 2013.

[4] Society of Automotive Engineers. J3016: Taxonomy and Definitions for Terms Related to Driving Automation Systems for On-Road Motor Vehicles. Standard, June 2018.

[5] L. C. Davis. Effect of adaptive cruise control systems on traffic flow. *Physical Review E*, 69(6):066110, 2004.

[6] R. Herman and R. B. Potts. Single lane traffic theory and experiment. In *Proceedings of the symposium on the theory of traffic flow*, pages 120–146, 1959.

[7] D. C. Gazis, R. Herman, and R. B. Potts. Car-following theory of steady-state traffic flow. *Operations Research*, 7(4):499–505, 1959.

[8] R. E. Chandler, R. Herman, and E. W. Montroll. Traffic dynamics: studies in car following. *Operations Research*, 6(2):165–184, 1958.

[9] V. Milanés and S. E. Shladover. Modeling cooperative and autonomous adaptive cruise control dynamic responses using experimental data. *Transportation Research Part C: Emerging Technologies*, 48:285–300, 2014.

[10] G. Gunter, C. Janssen, W. Barbour, R. E. Stern, and D. B. Work. Model based string stability of adaptive cruise control systems using field data. *Submitted to IEEE Transactions on Intelligent Vehicles*, 2019, under review.

[11] G. Gunter, D. Gloudemans, R. E. Stern, S. McQuade, R. Bhadani, M. Bunting, M. L. Delle Monache, R. Lysecky, B. Seibold, J. Sprinkle, B. Piccoli, and D. B. Work. Are commercially implemented adaptive cruise control systems string stable? *Submitted to IEEE Transactions on Control Systems Technology*, 2019, under review.

[12] J. Treiterer. Investigation of traffic dynamics by aerial photogrammetry techniques. Final Report EES278. *Transportation Research Center, Department of Civil Engineering, Ohio State University*, 1975.

[13] B. G. H. Gorte, F. K. Nejadasl, and S. P. Hoogendoorn. Outline extraction of motorway from helicopter image sequence. *CMRT, IAPRS Vienna*, 2005.

[14] M. Treiber, A. Hennecke, and D. Helbing. Congested traffic states in empirical observations and microscopic simulations. *Physical Review E*, 62(2):1805, 2000.

[15] ISO 15622. Intelligent transport systems–adaptive cruise control systems–performance requirements and test procedures, 2010.

[16] C.-Y. Liang and H. Peng. Optimal adaptive cruise control with guaranteed string stability. *Vehicle System Dynamics*, 32(4-5):313–330, 1999.

[17] V. Milanés, S. E. Shladover, J. Spring, C. Nowakowski, H. Kawazoe, and M. Nakamura. Cooperative adaptive cruise control in real traffic situations. *IEEE Transactions on Intelligent Transportation Systems*, 15(1):296–305, 2014.

[18] P. Seiler, A. Pant, and K. Hedrick. Disturbance propagation in vehicle strings. *IEEE Transactions on automatic control*, 49(10):1835–1842, 2004.